

# Optimal Generation of Pulsed Entangled Photon Pairs

Juan F. Hodelin,\* George Khoury, and Dirk Bouwmeester  
*Department of Physics, University of California, Santa Barbara, CA 93106, USA*  
(Dated: June 18, 2021)

We experimentally investigate a double-pass parametric down-conversion scheme for producing pulsed, polarization-entangled photon pairs with high visibility. The amplitudes for creating photon pairs on each pass interfere to compensate for distinguishing characteristics that normally degrade two-photon visibility. The result is a high-flux source of polarization-entangled photon pulses that does not require spectral filtering. We observe quantum interference visibility of over 95% without the use of spectral filters for 200 femtosecond pulses, and up to 98.1% with 5 nm bandwidth filters.

## I. INTRODUCTION

Quantum entanglement is one of the most striking concepts in quantum physics, and has now become the primary resource in the fields of quantum communication and quantum computation. Quantum information systems utilize entanglement to transmit, encode, and process data stored on qubits. For quantum communication protocols the natural candidate for a qubit is the photon. Qubits encoded in photons can fly freely through space or travel over optical fibers for long distances without decoherence.

Time of arrival [1, 2], spatial mode [3], and polarization [4, 5] are some of the degrees of freedom in which photons have been entangled. Polarization-entangled photon pairs have been produced using parametric down-conversion (PDC) reliably for almost two decades [4, 5]. A convenient source of polarization-entangled photons without the need for post-selection is non-collinear Type-II PDC [6]. These polarization-entangled photons have been used for many experiments including violations of Bell's inequality [6], quantum teleportation [7], quantum cloning [8], and quantum logic [9, 10, 11, 12]. A pulsed source of entangled photons is required for quantum information protocols for which well-defined timing is needed to interfere photons from different sources. This becomes important for experiments involving more than one pair of photons, such as entanglement swapping [13, 14].

There has been much work on designing sources of polarization-entangled photons that display high visibility quantum interference [15, 16, 17, 18, 19, 20, 21, 22, 23, 24, 25]. Sources pumped by continuous-wave (cw) lasers have demonstrated essentially perfect polarization visibility [15, 22, 25]. Sources pumped by ultrashort pulses, however, suffer from comparatively low visibility. In frequency space, the broader spectrum of a pulsed pump allows for the generation of down-converted photons whose color provides distinguishing information about the polarization. This correlation between polarization and frequency reduces the polarization visibility

[26, 27, 28]. Spectral filtering can be used to eliminate this distinguishing information, while a thin nonlinear crystal can be used to limit distinguishability *a priori*. Experiments that rely only on filtering or the use of thin nonlinear crystals can attain high visibility, but at lower photon count rates [29, 30, 31]. Another technique to compensate or correct for distinguishable information is the use of interference [32]. These schemes interfere distinguishable amplitudes by using two crystals [15, 17, 18, 19], combining photons at a beam-splitter [21, 25, 32], or overlapping two passes through the nonlinear crystal [16, 22, 23, 24]. We demonstrate a scheme which utilizes the third concept. The amplitudes to produce a distinguishable (or non-maximally entangled) photon pair in each pass are interfered to yield highly entangled states.

Recently, it has been demonstrated that reflecting the pump pulse and down-converted photon pair back through the nonlinear crystal stimulates the production of another photon pair in the same mode as the first [33]. This double-pass set-up has generated four-photon states used to demonstrate spin-1 singlet states [34] and heralded generation of path-entangled states [35], and additionally to investigate entangled modes of up to 100 photons [36]. Until now the properties of the two-photon state produced by the Type-II non-collinear double-pass have not been explored. In this paper we explain how this double-pass set-up can be used to optimally generate pulsed entangled photon pairs by effectively compensating all distinguishing information. Using the double-pass to interfere distinguishable pair amplitudes we demonstrate 95.6% visibility quantum interference for 200 femtosecond pulses without the use of narrowband filters, as well as 98.1% visibility with 5 nm bandwidth interference filters. In addition, this purification scheme allows correlated photons emitted in all directions to be collected as polarization-entangled photons. We conclude by examining the space-time visibility of the set-up and the effects on multiphoton states.

## II. VISIBILITY AND COMPENSATION BACKGROUND

The quantum interference visibility we refer to is the polarization visibility, and it is a common measure of the

---

\*corresponding author: hodelin@physics.ucsb.edu

quality of a polarization-entangled state. In the frame of the lab the nonlinear crystal always produces horizontally and vertically polarized photons, thus the visibility in this basis (HV) is high regardless of entanglement. By measuring the correlations in the plus and minus 45 degree linear (PM) and right and left circular (RL) polarization bases the quantum entanglement of the state can be determined. The polarization visibility, as defined here, is

$$V = \frac{X_a Y_b + Y_a X_b - X_a X_b - Y_a Y_b}{X_a Y_b + Y_a X_b + X_a X_b + Y_a Y_b}. \quad (1)$$

Here  $X_a Y_b$  is the number of coincidence counts measured between spatial modes  $a$  and  $b$  having polarizations  $X$  and  $Y$  respectively, which correspond to HV, PM, or RL depending on the measurement basis. It should be noted that  $|V| \leq 1$ . So, for example, the  $\phi^+$  Bell state has  $V = -1$  in the HV basis and the  $\psi^-$  Bell state has  $V = +1$  in all bases.

Before describing our specific experiment we should first explain what needs to be compensated or filtered to create maximally-entangled polarization states. In general we would like to be able to factorize the polarization from the other degrees of freedom (such as k-vector and frequency). When that is possible, gaining information about these observables will not provide any polarization information. This is not generally the case for photon pairs emitted from a Type-II source. Due to birefringence there is a temporal delay between the photons in each mode, and the extraordinary mode walks-off through the crystal along the optical axis. These temporal and spatial walk-offs can be effectively eliminated by using compensating crystals as in Ref. [6].

A new problem arises when the crystal is pumped by a broadband laser: the dispersion and phase-matching conditions in the nonlinear crystal create differences in the ordinary and extraordinary spectral modes [26, 27, 28]. In the case of  $\beta$  - barium borate (BBO) the spectrum of the ordinary photons is wider than that of the extraordinary photons. This disparity increases for increasing pump bandwidth. When using Type-II non-collinear PDC sources both spatial modes  $a$  and  $b$  (defined by the intersection of the well-known rings [6]) receive both extraordinary and ordinary photons. Thus, in principle, the polarization of the photon in each mode can be determined solely by knowledge of its frequency.

In the following we concentrate on spectral mode distinguishability. As mentioned above, the spectra of the down-converted photons can be made indistinguishable by filtering tightly, however this causes the photon count rates to decrease as well. Following a calculation by Grice and Walmsley [26], the polarization visibility and coincidence count rate can be obtained as functions of the filter bandwidth. Figure 1 shows these functions for typical crystal and pump laser parameters in our experiments. The visibility without filters is 62.2%, but this can be improved to 90.8% by using 5 nm bandwidth filters centered at 780 nm. If one would like to obtain 95%

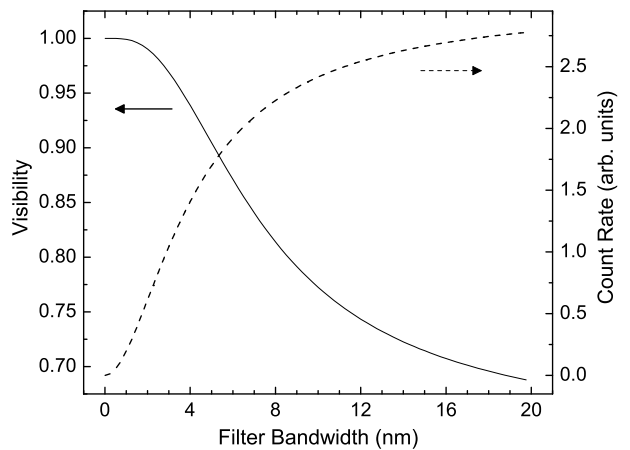


FIG. 1: Visibility and coincidence count rate as a function of filter bandwidth. This graph is for a 2 mm thick BBO crystal with the optical axis at 45 degrees to the pump. The pump has a Gaussian profile with full width half-max of 1 nm around 390 nm, and the down-converted photons are degenerate around 780 nm. The filter bandwidth is the half-width at  $1/e$  max.

visibility, then the count rate will be half of the unfiltered rate (assuming filters with ideal peak transmission).

Another technique to eliminate the spectral mismatch is the use of a thin nonlinear crystal to increase phase-matching (e.g., length  $< 0.5$  mm for our experimental parameters). This results in both extraordinary and ordinary photons having identical, broad spectra (FWHM  $> 15$  nm). The use of a thin crystal (100  $\mu\text{m}$ ) has been demonstrated to give high visibility fringes ( $V \simeq 98\%$ ), however the resulting coincidence count rates were below 100 Hz [31]. More recent experiments have attained much higher count rates using a thin crystal pumped by a cw laser [37].

A number of experiments have utilized interference in order to compensate PDC [15, 16, 17, 18, 19, 20, 21, 22, 23, 24, 25]. The first proposal for such a technique was by Kwiat, *et al.* who suggested using a half-waveplate and polarizing beam-splitter (PBS) to combine the output of two Type-II collinearly phase-matched down-converters [32]. This technique, combining photons at a PBS, is the one of three general types of interference compensation schemes. The others are overlapping the emission amplitudes of two nonlinear crystals and reflecting the down-converted photons and pump back through the nonlinear crystal. The first two techniques have proven quite effective by demonstrating visibility between 90-92% for ultrashort pulses without the use of spectral filters [17, 18, 20, 21]. The pulsed, double-pass schemes reported [16, 24] also increase visibility to 64% and 80%, respectively, without filtering. Specific comparisons become difficult due to the various types of measurements performed and the different experimental conditions (e.g., phase-matching, pump pulse length, crystal length). The double-pass scheme presented here provides

high visibility for unfiltered pulses without the need to post-select, while using the same set-up that has reliably produced multiphoton entangled states [33, 34, 35, 36]. In the following section we discuss the theory behind the double-pass compensation scheme employed in our experiment.

### III. THEORETICAL MODEL

To explain how the double-pass scheme interferes distinguishable amplitudes to produce a higher visibility state we present a simplified version of the detailed theory for PDC. Typically one begins with the effective interaction Hamiltonian for Type-II non-collinear single-pass PDC

$$\begin{aligned} H_{\text{Int}}(t) = & \\ & i\hbar\kappa \iint d\omega_o d\omega_e (\hat{a}_h^\dagger(\omega_o)\hat{b}_v^\dagger(\omega_e) - \hat{a}_v^\dagger(\omega_e)\hat{b}_h^\dagger(\omega_o)) \\ & \times f(\omega_o, \omega_e) + h.c. \end{aligned} \quad (2)$$

where  $f(\omega_o, \omega_e)$  is the joint spectral amplitude function [16, 26, 27, 28]. The interaction parameter,  $\kappa$ , depends on the pump intensity, the crystal's  $\chi^{(2)}$  nonlinearity, and the crystal length.

This detailed approach can be somewhat cumbersome, and a simpler technique is to ignore frequency correlations between photons. The frequency correlations do not affect the two-photon visibility, however they do become important when using more than one photon pair [38]. Ignoring frequency correlations means that  $f(\omega_o, \omega_e) = g(\omega_o)h(\omega_e)$ , and the frequency integrals above can be evaluated separately resulting in

$$H_{1\text{pass}} = i\hbar\kappa(\hat{a}'_h^\dagger\hat{b}'_v^\dagger - \hat{a}'_v^\dagger\hat{b}'_h^\dagger) + h.c. \quad (3)$$

The prime indicates that the ordinary photons are emitted into a different spectral mode than the extraordinary photons. The prime mode can be decomposed as  $\hat{a}' = x\hat{a}_1 + \sqrt{1-|x|^2}\hat{a}_2$  where modes 1 and 2 are orthogonal ( $[\hat{a}_1, \hat{a}_2^\dagger] = 0$ ). This characterizes the partial overlap between the ordinary and extraordinary spectral modes parameterized by the value of  $x$  (the only parameter of this simplified model). For the remainder of the paper we take ‘‘ordinary’’ and ‘‘extraordinary’’ to label *spectral modes* rather than polarization modes. The Hamiltonian can then be written

$$\begin{aligned} H_{1\text{pass}} = & i\hbar\kappa[x(\hat{a}_{h1}^\dagger\hat{b}_{v1}^\dagger - \hat{a}_{v1}^\dagger\hat{b}_{h1}^\dagger) \\ & + \sqrt{1-|x|^2}(\hat{a}_{h2}^\dagger\hat{b}_{v1}^\dagger - \hat{a}_{v1}^\dagger\hat{b}_{h2}^\dagger)] + h.c. \end{aligned} \quad (4)$$

The visibility of the photon pairs generated from such a Hamiltonian will be perfect ( $V=1$ ) in the HV basis. In the PM and RL polarization bases, however, the visibility will be limited to  $x^2$ . The second term does not contribute to the visibility because the terms  $a_{h2}b_{v1}$  and  $a_{v1}b_{h2}$  will not interfere when measured in the PM or RL

basis. Although the value of  $x$  can only be predicted by the more detailed theory, Eq. (4) conveniently explains the features of the double-pass as described below.

The effect of the double-pass is to add another set of modes, 3 and 4. These are analogs to 1 and 2, distinguished only by their time of arrival at the detectors. The polarization of the down-converted photons from the first pass is flipped ( $H \rightleftharpoons V$ ) before they are reflected back into the crystal (Fig. 2). The resulting Hamiltonian reads

$$\begin{aligned} H_{2\text{pass}} = & i\hbar\kappa \left[ x(\hat{a}_{v1}^\dagger\hat{b}_{h1}^\dagger - \hat{a}_{h1}^\dagger\hat{b}_{v1}^\dagger) \right. \\ & + \sqrt{1-|x|^2}(\hat{a}_{v2}^\dagger\hat{b}_{h1}^\dagger - \hat{a}_{h1}^\dagger\hat{b}_{v2}^\dagger) \\ & + e^{i\omega\Delta t} \left( x(\hat{a}_{h3}^\dagger\hat{b}_{v3}^\dagger - \hat{a}_{v3}^\dagger\hat{b}_{h3}^\dagger) \right. \\ & \left. \left. + \sqrt{1-|x|^2}(\hat{a}_{h4}^\dagger\hat{b}_{v3}^\dagger - \hat{a}_{v3}^\dagger\hat{b}_{h4}^\dagger) \right) \right] + h.c., \end{aligned} \quad (5)$$

where  $\omega$  is the frequency of the pump laser, and  $\Delta t$  is the difference in arrival times of the two passes at the detectors. The change in polarization labels on the first pass can alternatively be viewed as an exchange of the spectral-mode labels ( $1 \rightleftharpoons 2$ ). When  $\Delta t$  is much less than the coherence time of the down-converted photons, modes 1 and 3 are equivalent, and modes 2 and 4 are equivalent. The Hamiltonian can then be written

$$\begin{aligned} H_{2\text{pass}}^{\Delta t \simeq 0} = & i\hbar\kappa \left[ x(1 + e^{i\theta})(\hat{a}_{h1}^\dagger\hat{b}_{v1}^\dagger - \hat{a}_{v1}^\dagger\hat{b}_{h1}^\dagger) \right. \\ & + \sqrt{1-|x|^2} \left( (e^{i\theta}\hat{a}_{h2}^\dagger\hat{b}_{v1}^\dagger - \hat{a}_{v2}^\dagger\hat{b}_{h1}^\dagger) \right. \\ & \left. \left. + (\hat{a}_{h1}^\dagger\hat{b}_{v2}^\dagger - e^{i\theta}\hat{a}_{v1}^\dagger\hat{b}_{h2}^\dagger) \right) \right] + h.c., \end{aligned} \quad (6)$$

where  $\theta = \omega\Delta t$  is the relative phase of the two passes. Rotating the polarization of the first pass and overlapping it with the second pass creates a coherent superposition of down-converting in each pass. The first pass provides ordinary V-polarized photons and extraordinary H photons, while the second pass creates ordinary H and extraordinary V photons. When both passes are combined, knowing the spectral mode no longer provides any polarization information. This is equivalent to symmetrizing  $f(\omega_o, \omega_e)$  with respect to interchanging its arguments [16]. Through this technique we optimally compensate the spectral mismatch of pulsed PDC.

Notice that the first term of Eq. (6) can be stimulated (or suppressed) as a function of the phase ( $\theta$ ). The other terms have a constant amplitude since the phase appears inside these terms. When the phase is equal to zero, the state produced by Eq. (6) is a superposition of three  $\psi^-$  Bell states, each with visibility equal to one.

Even from this simple, two-mode model it becomes evident that this technique only works perfectly on two-photon, PDC events [39]. Multiphoton events ( $n > 2$ ) result from the higher-order terms of the interaction Hamiltonian. Exponentiating the Hamiltonian mixes the modes such that the spatial and spectral mode labels again become distinct. For the simplest example, consider the second-order (four-photon) state. Once Eq. (6)

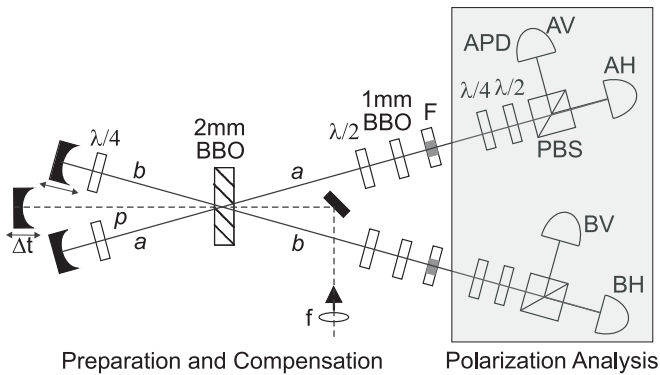


FIG. 2: Experimental set-up. The pump beam (dotted line) is focused by a lens ( $f$ , focal length = 50 cm), and passes through the nonlinear crystal (BBO) twice with a variable delay. The down-converted photons (solid line) from the first pass have their polarization rotated by 90 degrees by twice traversing  $\lambda/4$  waveplates at 45 degrees. After the second pass the photons are compensated for walk-off (see Fig. 3) and filtered (F) before entering single-mode fibers for polarization analysis.

is squared only the terms that square with themselves remain maximally entangled; the cross terms are multimode in the spectral mode space. Nonetheless, the double-pass scheme does mitigate the spectral mismatch, and multiphoton experiments using this set-up have reported four-photon visibilities over 80% [35]. The primary source of decoherence in those experiments was distinguishable temporal modes imparted by the short down-converted pulse length compared to that of the pump pulse [38, 40].

## IV. EXPERIMENTAL DEMONSTRATION

### A. Double-Pass Set-Up

To test the double-pass compensation scheme we utilized a slightly modified version of the design of Ref. [33]. A frequency-doubled, Ti:Sapphire laser operating at 82 MHz repetition rate provides 200 fs pulses centered at 390 nm. As illustrated in Fig. 2 these pulses are focused onto a 2 mm thick BBO crystal where PDC takes place. The pump pulse and down-converted photons leave the crystal in distinct spatial modes  $p$ ,  $a$ , and  $b$ . Each mode is aligned normal to the center of a curved mirror, which reflects the modes back into the crystal along their same paths. Modes  $p$  and  $b$  are each on translation stages so that the arrival time of all three modes can be matched at the crystal. Quarter-waveplates oriented at 45 degrees are placed into modes  $a$  and  $b$ . These flip the polarization of the first-pass photon amplitudes when traversed twice. When the timing of  $p$ ,  $a$ , and  $b$  match, these amplitudes interfere with those of creating a photon pair in the second pass to create the two-photon, high-visibility state of Eq. (6).

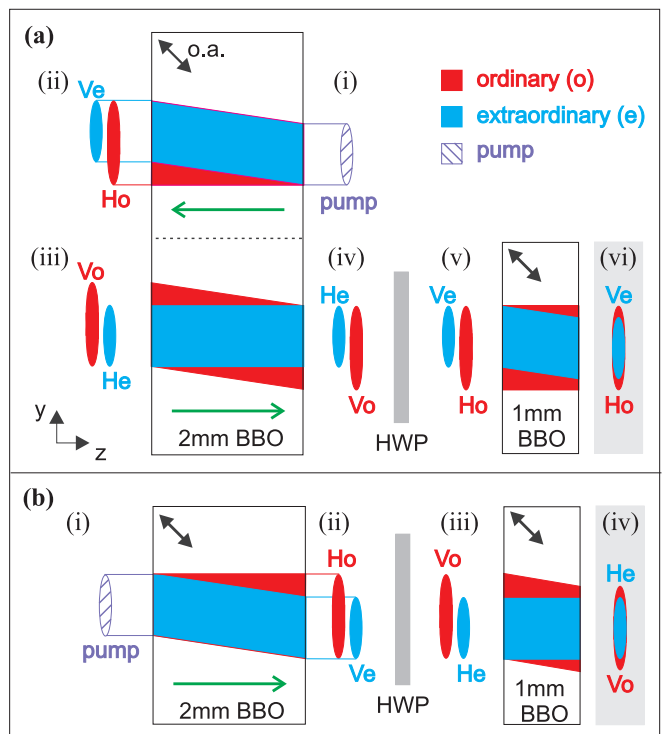


FIG. 3: (Color online) Walk-off compensation. Long arrows indicate direction of beam propagation. The shaded boxes depict the final states for each pass. (a) Compensation of photons created in the first pass. (i) The vertically-polarized pump beam walks off along the optical axis (o.a.) of the 2 mm crystal creating down-converted photons along its entire length. The V-polarized, extraordinary ( $e$ ) photons walk with the pump beam, while the H-polarized, ordinary ( $o$ ) photons continue along the  $z$ -axis. (ii) The resulting  $o$  spatial profile is stretched along the  $y$ -axis (perpendicular to optical table) and lags behind in space-time ( $z$ -axis) by 1 mm of birefringence on average. (iii) The net effect of twice traversing the quarter-waveplates and reflecting from the curved mirrors (not shown) is to flip the polarizations and invert the spatial profiles. (iv) The second trip through the 2 mm crystal (shifted for clarity) walks the V-polarized,  $o$  photons along the o.a. They also emerge ahead in time. (v) A HWP flips the polarizations. (vi) A 1 mm BBO crystal overlaps the  $o$  and  $e$  photons together in space and time. (b) Second-pass photon compensation. (i) The pump pulse passes through the 2 mm BBO a second time (ii) generating down-converted photons. (iii) A HWP flips polarizations. (iv) The 1 mm BBO again overlaps the  $o$  and  $e$  photons. Notice that the final state of the first pass photons corresponds to that of the second pass, however the polarizations are interchanged.

After the second pass through the crystal, modes  $a$  and  $b$  pass through half-wave plates at 45 degrees and 1 mm BBO crystals to correct for spatial and temporal walk-off. The entire walk-off compensation scheme is shown schematically in Fig. 3, and is described in detail in the figure caption. The result is that photons from the first pass with swapped mode labels are completely indistinguishable from those produced in the second pass with

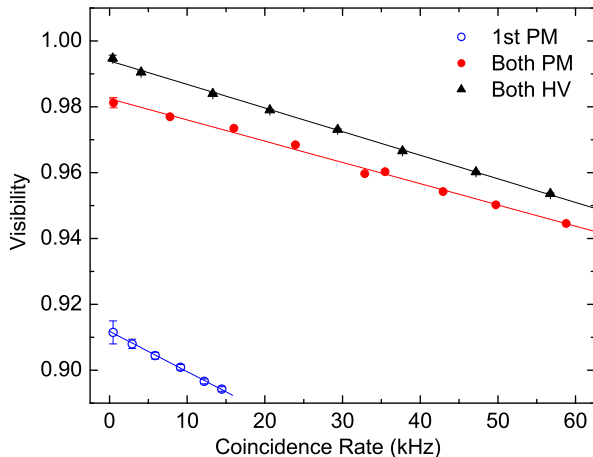


FIG. 4: (Color online) Visibility as a function of coincidence count rate with 5 nm bandwidth filters. The visibility decreases linearly as the pump power is increased in both HV (triangles) and PM (circles) bases due to increasing noise from four-photon, down-conversion events. Record high visibilities for pulsed down-conversion of up to 98.1% are shown in the PM basis using the double-pass; an improvement of 7.0% over the 1st pass alone. The highest count rates correspond to a pump power of 400 mW.

normal mode labels. The temporal profiles overlap and the spatial profiles are centered to facilitate equal fiber coupling. Once the photons are properly compensated, depending on the measurement being performed, they are filtered spectrally with narrowband or edgepass filters and spatially with single-mode fibers. The visibility is measured using the polarization analysis set-up consisting of a quarter-waveplate, half-waveplate, and polarizing beam-splitter (PBS). The light is detected by avalanche photodiodes (APDs) connected to a coincidence logic circuit with a window of 2 ns.

Mode distinguishability is not the only source of decreased visibility. More than one PDC event may take place per pump pulse with an amplitude proportional to the interaction parameter  $\kappa^n$  for  $n$  pair events. These events can degrade the two-photon visibility [36]. This, however, has a smaller effect on the visibility than mode distinguishability at the pump powers used in our experiment. For small values of  $\kappa$  the contribution from four-photon events is the dominant noise term, and the visibility decreases linearly. The visibility data presented in this paper depicts this trend showing a typical 4-8% visibility decrease as the pump power is increased by a factor of order 100.

## B. Spectral Compensation Results

The spectral compensation was tested experimentally by comparing the visibility of the individual passes to that of the double-pass with and without narrowband fil-

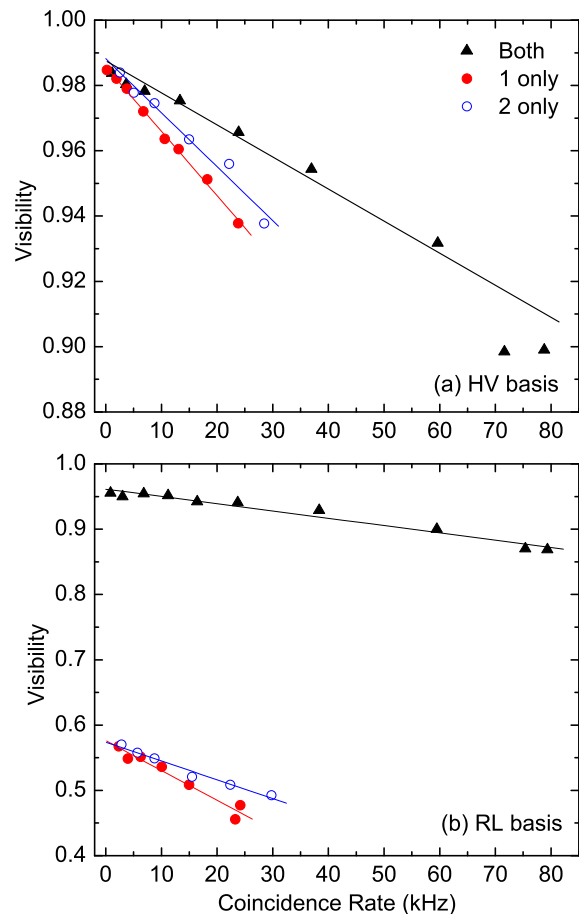


FIG. 5: (Color online) Visibility as a function of coincidence count rate with only edgepass filtering. The data displayed is for each pass individually (circles) and both passes combined (triangles). Lines are provided to guide the eye. (a) HV basis. The visibility is high in all three cases, and decreases at higher power due to noise from four-photon events. (b) RL basis. The double-pass vastly improves the visibility from around 55% for single passes to over 95%. Error bars are smaller than the height of the symbols. The highest count rates correspond to a pump power of 300 mW.

ters. The single-pass visibility is given by  $x^2$ , which can be determined by calculation [26], or by directly measuring the visibility of a single pass. The  $x^2$  values listed below are determined by measurement, but they are in good agreement with theory (cf. Fig. 1). The double-pass visibility predicted by Eq. (6) should be equal to one at phase equal to zero, regardless of  $x$ .

When using narrowband filters the spectral modes are governed by the convolution of the ordinary and extraordinary spectral profiles with those of the filters, and are therefore almost indistinguishable, ( $x^2 = .91$ ). The visibility of the double-pass with 5 nm filters as a function of the coincidence count rate is shown in Fig. 4. The count rate was decreased by rotating the pump polarization in steps, which reduced the pump power along the optical

axis of the crystal. A maximum visibility of  $98.1 \pm 0.15\%$  in the PM basis is considerably higher than the 91% predicted and measured for a single-pass. The count rate at this point is 519 Hz. The double-pass also allows high count rates and visibility simultaneously by displaying over 50000 coincidences per second with 95% visibility. This corresponds to over five million entangled photon pairs per second produced by the crystal when our 10% collection efficiency is considered.

When only edgepass filters are used to eliminate residual UV light from the pump beam, the ordinary and extraordinary spectra differ and the value of  $x$  is small ( $x^2 \approx .57$ ). This can be seen in the RL visibility of the individual passes in Fig. 5(b). The individual pass visibilities peak at 57%, however by interfering these same two passes the visibility jumps as high as  $95.6 \pm 0.45\%$  at a rate of 855 Hz. The double-pass has effectively eliminated the spectral distinguishability without having to sacrifice photons to lossy narrowband filters.

### C. Spatial Compensation

To this point we have focused on the double-pass compensating the spectral mismatch, however this scheme works comparably well in eliminating spatial-mode mismatch. To verify this we aligned the collection optics such that modes  $a$  and  $b$  corresponded to conjugate points slightly away from the intersection of the rings. This varies the amplitude of the individual terms ( $a_h b_v$  and  $a_v b_h$ ) in each pass, parameterized by  $y$  below

$$H_{\text{misalign}} = i\hbar\kappa \left[ (y\hat{a}_{h1}^\dagger \hat{b}_{v1}^\dagger - \sqrt{1-y^2}\hat{a}_{v1}^\dagger \hat{b}_{h1}^\dagger) + e^{i\omega t} (y\hat{a}_{v2}^\dagger \hat{b}_{h2}^\dagger - \sqrt{1-y^2}\hat{a}_{h2}^\dagger \hat{b}_{v2}^\dagger) \right] + h.c. \quad (7)$$

Mode 1 labels the first pass through the crystal, and 2 the second, where the same misalignment,  $y$ , is assumed for both. Here we have ignored the spectral differences parameterized by  $x$ , but it is trivial to show that compensation holds given both spatial and spectral mismatch.

If the passes overlap in time, then they can interfere and produce an entangled state upon leaving the crystal the second time

$$H_{\text{misalign}}^{\Delta t \simeq 0} = i\hbar\kappa \left[ y(\hat{a}_h^\dagger \hat{b}_v^\dagger + e^{i\theta}\hat{a}_v^\dagger \hat{b}_h^\dagger) - \sqrt{1-y^2}(e^{i\theta}\hat{a}_h^\dagger \hat{b}_v^\dagger + \hat{a}_v^\dagger \hat{b}_h^\dagger) \right] + h.c. \quad (8)$$

Once again the two passes have been interfered to produce a Bell state with  $|V| = 1$ , regardless of the value of  $y$ . This means that even if the crystal only emits  $a_h b_v$  ( $y = 1$ ) in a single pass, maximal entanglement can still be obtained with the double-pass. All conjugate points of the Type-II rings can be collected as sources of polarization-entangled photons, rather than just the intersection of the rings. This allows for an increase in photon flux while preserving high visibility (for instance, with the use of multimode collection).

To verify this experimentally, the count rates of the individual passes were aligned to two different  $y$  values:  $y^2 = .28$  and  $y^2 = .12$ . The average single-pass visibilities at these points were 47.9% and 23.5%, respectively, with 5 nm interference filters. When both passes were combined, the measured visibility jumped to 94.2% and 91.8%, respectively, in the PM basis. Similar results were obtained in the RL basis. Coincidence count rates were over 5000 Hz for both measurements. These high visibilities indicate that substantial polarization entanglement exists for any photons with correlated k-vectors emitted from the crystal.

## V. SPACE-TIME VISIBILITY

So far we have restricted our definition of visibility to polarization visibility, obtained by comparing the signal of terms consistent with the state desired to noise from unwanted terms. Another type of measurement that can be done with the double-pass is the space-time, or path visibility. This is the visibility of the fringes obtained when the pump mirror is translated along the axis of the pump beam. This varies the phase between the two passes, that is  $\theta$  of Eq. (6), resulting in sinusoidal oscillations in the down-converted, photon-pair intensity.

Using the simple model described in Section III predictions can also be made for the path visibility for given values of  $x$  and  $y$ . We consider a well-aligned set-up with imperfect filtering ( $y = 1, x < 1$ ). Interestingly, when the polarization is analyzed in the HV basis the path visibility is limited to  $x^2$ , but when analyzed in the PM or RL bases the visibility is one, regardless of  $x$ . This feature of the system is elucidated by the simplified interaction Hamiltonian.

To see these properties consider Eq. (6) for  $x < 1$ . Of the three terms, only the first has a phase-dependent amplitude. This term oscillates as a function of phase to produce interference fringes. The other terms are phase independent, and therefore degrade the path visibility in the HV basis by providing a constant background of HV counts. It is easy to show that evaluating the HV fringe visibility with this constant background gives a maximum value of  $x^2$ . Upon rotating to the PM (or RL) basis all of the terms that contribute to the PM (RL) coincidences have a phase-dependent amplitude:  $(1 + e^{i\theta})$ . Therefore, the PM (RL) count rate is zero at  $\theta = n\pi$  (for odd integer  $n$ ) regardless of  $x$ , and the PM (RL) space-time visibility is one.

These features are illustrated in Fig. 6. Figure 6(a) shows the interference fringes of HV coincidences measured with narrowband filters ( $x^2 = .91$ ) and with edgepass filters ( $x^2 \approx .49$ ). The visibility is determined by a fit of the data with a sine-squared function. The HV fringe visibility is 91.3% with 5 nm filters compared to 48.2% with only edgepass. In contrast, the RL interference fringes (Fig. 6(b)) display 96.1% visibility with 5 nm filters and 92.4% with edgepass filters. Similar results

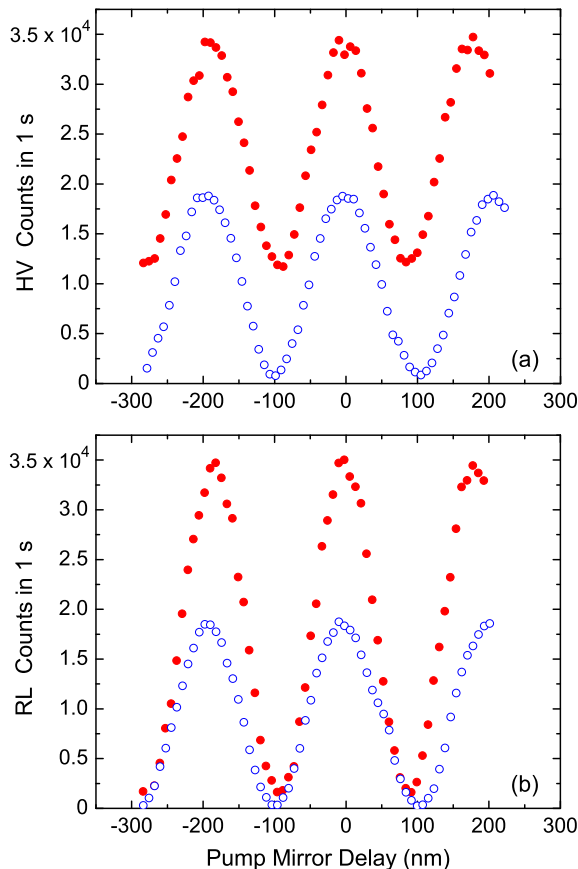


FIG. 6: (Color online) Space-time visibility for spatially aligned passes. The visibility is measured with 5 nm bandwidth filters (open circles) and edgepass filters (closed circles). In the (a) HV basis visibility is limited to  $x^2$ , however in the (b) RL basis the visibilities are close to the theoretical value of 1. The fringe visibility increases the closer the minima get to zero counts.

were obtained in the PM basis.

As predicted the visibility in the RL basis remains high regardless of the spectral-mode distinguishability (value of  $x$ ), while in HV it goes as  $x^2$ . These fringe visibilities are affected adversely by multiple-pair events in a similar manner as the polarization visibility. This limits the maximum visibilities in all bases as a function of the interaction parameter and detection efficiencies.

## VI. SUMMARY AND DISCUSSION

While the double-pass scheme has many advantages, a serious challenge is the required interferometric stability. Unlike four-photon experiments with the double-pass [33, 34, 35], the phase does not just modulate the intensity of the state, but also the phase within some

terms (see Eq. (6)). This means that not only does the signal decrease away from  $\theta = 0$ , but the state produced contains components that are not  $\psi^-$  states. Typical stability periods before the interferometer would drift approximately 3% from the maximum, were around 2 minutes in an environment partially isolated from external vibrations. All polarization visibility data was collected at spatial-fringe maxima for intervals shorter than this period. A clever technique to increase stability is to replace the three separate curved mirrors with a single, large curved mirror with high reflectivity at both the pump and down-converted photon wavelengths. This has been demonstrated for a Type-I non-collinear geometry in Ref. [22, 23]. This single-arm interferometer then makes it possible to build a reference interferometer as in Ref. [16] for active stabilization.

We have presented the theory and experimental results for a double-pass compensation scheme for pulsed parametric down-conversion. A simplified Hamiltonian was introduced to explain the form of the down-converted state with and without compensation. When the passes overlap the amplitudes for normally labelled photons and those with switched labels become indistinguishable, thereby optimally compensating any spectral and spatial-mode mismatch.

Using the double-pass scheme high polarization visibility was achieved without spectral filters (95.6%), and even higher (98.1%) with 5 nm bandwidth filters. The lower visibility without filters may have resulted from the reduced effectiveness of the optics with a broader spectrum of photons. The waveplates and compensating crystals no longer put the appropriate phases on photons as their wavelengths differ from 780 nm. Another possibility is the effect of group velocity dispersion, which was not considered in our model. Double-pass compensation is not limited to spectral-mode distinguishability. Spatial-mode mismatch was eliminated by combining single passes with an average visibility of 23.5% to attain over 92% visibility.

In addition to these demonstrations, we verified a prediction about the space-time visibility based on the simplified theory. In contrast to polarization visibility, the space-time visibility measured in the HV basis is reduced by spectral mismatch, while the visibility remains one for the complementary PM and RL bases. The space-time and spatial-mode mismatch visibilities were limited primarily by two-pair, down-conversion events, since this data was taken only at high pump power.

This research has been supported by NSF Grant No. 0304678 and by the DARPA MDA 972-01-1-0027 grant. J.F.H. thanks Lucent Technologies CRFP for financial support. We acknowledge support from Perkin-Elmer regarding the SPCM-AQR-13-FC single-photon counting modules.

- 
- [1] J. D. Franson, Phys. Rev. Lett. **62**, 2205 (1989).
- [2] J. Brendel, N. Gisin, W. Tittel, and H. Zbinden, Phys. Rev. Lett. **82**, 2594 (1999).
- [3] J. G. Rarity and P. R. Tapster, Phys. Rev. Lett. **64**, 2495 (1990).
- [4] Z. Y. Ou and L. Mandel, Phys. Rev. Lett. **61**, 50 (1988).
- [5] Y. H. Shih and C. O. Alley, Phys. Rev. Lett. **61**, 2921 (1988).
- [6] P. G. Kwiat, *et al.*, Phys. Rev. Lett. **75**, 4337 (1995).
- [7] D. Bouwmeester, *et al.*, Nature (London) **390**, 575 (1997).
- [8] A. Lamas-Linares, C. Simon, J.C. Howell, and D. Bouwmeester, Science **296**, 712 (2002).
- [9] K. Sanaka, T. Jennewein, J.-W. Pan, K. Resch, and A. Zeilinger, Phys. Rev. Lett. **92**, 017902 (2004).
- [10] S. Gasparoni, J.-W. Pan, P. Walther, T. Rudolph, and A. Zeilinger, Phys. Rev. Lett. **93**, 020504 (2004).
- [11] P. Walther *et al.*, Nature (London) **434**, 169 (2005).
- [12] N. Kiesel, *et al.*, Phys. Rev. Lett. **95**, 210502 (2005).
- [13] M. Zukowski, A. Zeilinger, M. A. Horne, and A. K. Ekert, Phys. Rev. Lett. **71**, 4287 (1993).
- [14] J.-W. Pan, D. Bouwmeester, H. Weinfurter, and A. Zeilinger, Phys. Rev. Lett. **80**, 3891 (1998).
- [15] P. G. Kwiat, E. Waks, A. G. White, I. Appelbaum, and P. H. Eberhard, Phys. Rev. A **60**, R773 (1999).
- [16] D. Branning, W. P. Grice, R. Erdmann, and I. A. Walmsley, Phys. Rev. Lett. **83**, 955 (1999); Phys. Rev. A **62**, 013814 (2000).
- [17] Y.-H. Kim, S.P. Kulik, and Y. Shih, Phys. Rev. A **62**, 011802(R) (2000); Y.-H. Kim, S. P. Kulik, and Y. Shih, *ibid.* **63**, 060301 (2001).
- [18] Y.-H. Kim, S. P. Kulik, and Y. Shih, Phys. Rev. A **62**, 011802(R) (2000).
- [19] G. Bitton, W. P. Grice, J. Moreau, and L. Zhang, Phys. Rev. A **65**, 063805 (2001).
- [20] Y. Nambu, K. Usami, Y. Tsuda, K. Matsumoto, and K. Nakamura, Phys. Rev. A **66**, 033816 (2002).
- [21] Y.-H. Kim, S. P. Kulik, M. V. Chekhova, W.P. Grice, Y. Shih, Phys. Rev. A **67**, 010301(R) (2003).
- [22] G. Giorgi, G. Di Nepi, P. Mataloni, and F. De Martini, Laser Physics **13**, 350 (2003).
- [23] M. Barbieri, F. De Martini, G. Di Nepi, and P. Mataloni, Phys. Rev. Lett. **92**, 177901 (2004).
- [24] B. S. Shi and A. Tomita, Opt. Commun. **235**, 247 (2004).
- [25] M. Fiorentino, G. Messin, C. E. Kuklewicz, F. N. C. Wong, and J. H. Shapiro, Phys. Rev. A **69**, 041801(R) (2004).
- [26] W. P. Grice and I. A. Walmsley, Phys. Rev. A **56**, 1627 (1997).
- [27] T. E. Keller and M. H. Rubin, Phys. Rev. A **56**, 1534 (1997).
- [28] Z. Y. Ou, Quantum Semiclassic. Opt. **9**, 599 (1997).
- [29] G. Di Giuseppe, L. Haiberger, F. De Martini, and A. V. Sergienko, Phys. Rev. A **56**, R21 (1997).
- [30] W. P. Grice, R. Erdmann, I. A. Walmsley, and D. Branning, Phys. Rev. A **57**, R2289 (1998).
- [31] A. V. Sergienko, *et al.*, Phys. Rev. A **60**, R2622 (1999).
- [32] P. G. Kwiat, P. H. Eberhard, A. M. Steinberg, and R. Y. Chiao, Phys. Rev. A **49**, 3209 (1994).
- [33] A. Lamas-Linares, J. C. Howell, and D. Bouwmeester, Nature (London) **412**, 887 (2001).
- [34] J. C. Howell, A. Lamas-Linares, and D. Bouwmeester, Phys. Rev. Lett. **88**, 030401 (2002).
- [35] H. S. Eisenberg, J. F. Hodelin, G. Khoury, and D. Bouwmeester, Phys. Rev. Lett. **94**, 090502 (2005).
- [36] H. S. Eisenberg, G. Khoury, G. Durkin, C. Simon, and D. Bouwmeester Phys. Rev. Lett. **93**, 193901 (2004).
- [37] P. S. K. Lee, M. P. van Exter, and J. P. Woerdman, Phys. Rev. A **70**, 043818 (2004).
- [38] W. P. Grice, A. B. URen, and I. A. Walmsley, Phys. Rev. A **64**, 063815 (2001).
- [39] The non-ideal compensation is evident from the simplified model, although the assumption in deriving that model (about being justified in ignoring frequency correlations) is invalid. The joint spectral amplitude function can no longer be assumed to be separable [38].
- [40] Z. Y. Ou, J. K. Rhee, L. J. Wang, Phys. Rev. A **60**, 593 (1999).